Annales
Geophysicae

Open Access

Observation of electron biteout regions below sporadic E layers at polar latitudes

G. A. Lehmacher[1]**, M. F. Larsen**[1]**, and C. L. Croskey**[2]

[1]Department of Physics & Astronomy, Clemson University, Clemson, SC, USA
[2]Department of Electrical Engineering, The Pennsylvania State University, University Park, PA, USA

Correspondence to: G. A. Lehmacher (glehmac@clemson.edu)

Abstract. The descent of a narrow sporadic E layer near 95 km altitude over Poker Flat Research Range in Alaska was observed with electron probes on two consecutive sounding rockets and with incoherent scatter radar during a 2 h period near magnetic midnight. A series of four trimethyl aluminum chemical releases demonstrated that the Es layer remained just slightly above the zonal wind node, which was slowly descending due to propagating long-period gravity waves. The location of the layer is consistent with the equilibrium position due to combined action of the wind shear and electric fields. Although the horizontal electric field could not be measured directly, we estimate that it was $\sim 2\,\mathrm{mV\,m^{-1}}$ southward, consistent with modeling the vertical ion drift, and compatible with extremely quiet conditions. Both electron probes observed deep biteout regions just below the Es enhancements, which also descended with the sporadic layers. We discuss several possibilities for the cause of these depletions; one possibility is the presence of negatively charged, nanometer-sized mesospheric smoke particles. Such particles have recently been detected in the upper mesosphere, but not yet in immediate connection with sporadic E. Our observations of electron depletions suggest a new process associated with sporadic E.

Keywords. Ionosphere (Auroral ionosphere; Ionospheric irregularities) – Meteorology and atmospheric dynamics (Instruments and techniques)

1 Introduction

The formation of long-lived, sporadic E layers (Es) has been an intriguing subject of aeronomy for decades. Whitehead (1961, 1970) and Axford (1963) developed the wind shear theory, in which ions are swept together by the combined action of neutral collisions and Lorentz force; for recent reviews see Mathews (1998) or Haldoupis (2011). Observation of persistent, narrow layers implies the important role of long-lived metallic ions (e.g., Fe^+, Mg^+, Si^+, Na^+, Ca^+), which are abundant in the upper mesosphere and lower thermosphere through meteor ablation. Improved sensitivity of experimental techniques, such as incoherent scatter radar (ISR), shows that sporadic layers with a variety of plasma densities, widths, and lifetimes are a common presence throughout the E region (e.g., Mathews, 1987, 1998; Turunen et al., 1993).

It was soon recognized that, near the magnetic equator and at high latitudes, the wind shear mechanism would not be as efficient as at mid-latitudes due to the small or large inclination of the magnetic field. At polar latitudes, convection electric fields often provide the important driver for convergence or divergence in the ion motion (Nygren et al., 1984; Turunen et al., 1993; Bristow and Watkins, 1991, 1993; Kirkwood and von Zahn, 1991, 1993; Kirkwood and Nilsson, 2000; Williams et al., 2006).

Through solving the equation of motion and neglecting terms with gravity, the vertical neutral wind and ion diffusion (e.g., Kirkwood and von Zahn, 1993; Williams et al., 2006), the vertical ion drift v_{iz} can be expressed by

$$v_{iz} = \frac{\cos I}{1 + \rho_i^2}\left(\frac{E_E}{B_0} - U_N \sin I\right) + \frac{\rho_i \cos I}{1 + \rho_i^2}\left(\frac{E_N}{B_0} + U_E\right), \quad (1)$$

where U_N, U_E, E_N, and E_E are the magnetic northward and eastward components of the neutral wind and electric field, respectively; I is the magnetic inclination; and $\rho_i = \nu_i/\omega_i$ the ratio of ion–neutral collision and ion gyro frequencies. The collision frequency increases exponentially with neutral

Table 1. Designations for turbopause payloads with launch times and azimuth (clockwise from north).

Time	Mission no.	Launch azimuth [deg]
09:59 UT	NASA 41.076	0.6
10:29 UT	NASA 41.078	0.0
10:59 UT	NASA 41.079	−6.4
11:49 UT	NASA 41.077	−0.3

density, and therefore the second term containing the zonal wind dominates the vertical ion drift below about 110 km altitude. In the absence of an electric field, the ion layer is observed to form near the zero in the zonal wind with a westward shear. However, it can also be seen that $\cos I$ is small for high inclination, and the wind alone is less efficient.

Many sporadic layers (again, disregarding electric fields) are formed by tidal winds, e.g., semidiurnal or diurnal modes, but gravity waves may provide additional wind nodes (Turunen et al., 1993). If the layer follows the zero wind node of an upward propagating gravity wave, it will descend in time. Eventually, collision frequencies become too large and diffusion processes "dump" the layer into the background ionosphere (Chimonas and Axford, 1968). Sporadic E layers are therefore rarely observed below 90 km.

The composition of the layers of metallic ions connects Es to meteor ablation processes (Hunten et al., 1980) and the formation of the neutral metal layers in the upper mesosphere (Kirkwood and von Zahn, 1991, 1993; Heinselman et al., 1998). The detection of neutral and charged meteoric smoke or dust particles in the mesosphere has become a very active field, and different rocket techniques have been deployed (e.g., Havnes et al., 1996; Croskey et al., 2004; Rapp et al., 2005; Lynch et al., 2005; Knappmiller et al., 2008).

Mathews (1987) discusses the possibility of electron attachment to dust particles from meteor ablation. While deep electron depletions in connection with large, icy dust particles near the polar summer mesopause are well known (e.g., Ulwick et al., 1988), Friedrich et al. (2012) observed electron loss in connection with dust layers also for winter nighttime conditions.

In this paper we report observations of sporadic E layers at high latitudes under geomagnetically very quiet conditions. The layers were observed by two rockets carrying fixed-bias Langmuir probes delivering very fine detail of the vertical plasma structure in the D and lower E region. A sequence of four rockets with trimethyl aluminium (TMA) releases provided measurements of the neutral wind in the upper mesosphere and lower thermosphere. The Poker Flat Incoherent Scatter Radar (PFISR) used five beams simultaneously adding some information about the time development and horizontal extent of the layers; however, electron densities were just above the observation threshold during this portion of the night when the rocket observations were made.

The primary goal of the experiment was the observation of the development of neutral turbulence around the turbopause (Lehmacher et al., 2011; Collins et al., 2011). Our observation of Es was incidental, but worthy of attention, since simultaneous measurements of Es and neutral winds are relatively rare, and accurate wind measurements are difficult to obtain in this region. Many studies have focused on mid-latitudes and events above 100 km, where strong layers are observed and the wind shear mechanism is most effective, sometimes modified by electric fields (e.g., MacLeod, 1966; Kato et al., 1972; Smith and Mechtly, 1972; Smith and Miller, 1980; Wakabayashi and Ono, 2005).

We focus on two key observations which we find significant for our case study of an Es at auroral latitude: (1) the close correlation between layer height and zonal wind shear node, and (2) deep electron depletions just below the layer of enhancement.

The paper is organized as follows: in Sect. 2 we briefly introduce the experimental techniques, in Sect. 3 we present the time development of wind profiles and layer altitude, and in Sect. 4 we discuss the electron depletion and possible reasons. In Sect. 5, we summarize our results.

2 Experiment

The NASA sounding rocket experiment Turbopause was conducted on 17–18 February 2009 at Poker Flat Research Range (PFRR), Alaska (64° N, 147° W). The magnetic inclination and declination angles are 77.41 and 24.89°. Local midnight is at 09:00 UT and magnetic midnight at 11:20 UT. The main purpose of the experiment was to study the transition from strong mixing and turbulence to more laminar behavior as visible in chemical trail releases. Results of the wind, temperature, and turbulence measurements were reported by Lehmacher et al. (2011), and a mixing event in the mesosphere observed in the sodium layer was studied by Collins et al. (2011).

Four two-stage Terrier-Improved Orion sounding rockets were launched within a 2 h period starting at 09:59 UT (00:59 LT) northward along similar trajectories. Neutral winds were measured by all four rockets with the TMA chemical release technique (Larsen, 2002). The second and third rocket carried additional instrumented daughter payloads measuring neutral parameters with the Combined Neutral and Electrons (CONE) ionization gauge (Giebeler et al., 1993), and negatively charged particles (electrons and negative ions) with dual fixed-bias Langmuir probes: a nose-tip probe at the front (Croskey et al., 2006) and the CONE instrument in the aft. The NASA payload designations and launch times are given in Table 1.

Figure 1 shows the proportions of the relatively short instrumented payload with a long, straight nose cone and the CONE sensor in the aft. Both instrumented rockets exited the lower atmosphere at relatively low body elevation angles
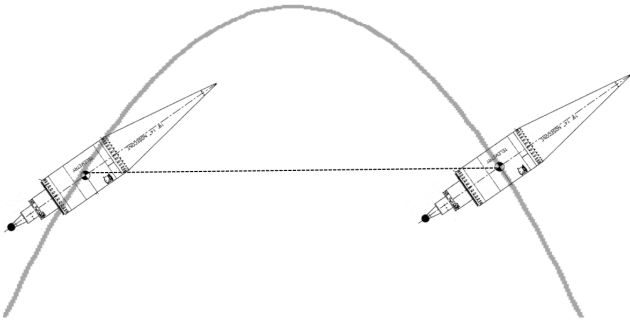
Figure 1. Orientation for payload 41.078 at 95 km upleg and downleg. The angle of attack (angle between roll axis and velocity vector) is critical for gas flow around instruments and plasma collection.
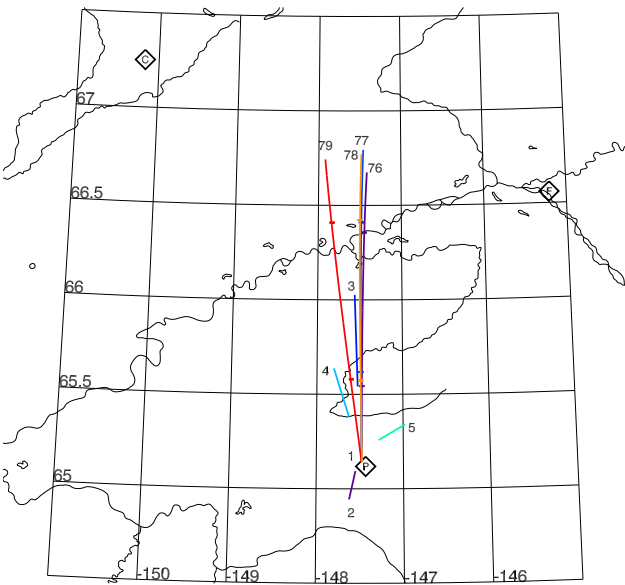

Figure 2. Four payload trajectories (76, 77, 78, 79) and five PFISR radar beams (1, 2, 3, 4, 5) projected on a map of central Alaska. The points of intersection at 95 km altitude on upleg and downleg are marked with a short dash. The diamonds indicate the launch site, Poker Flat (P), and the camera sites for TMA observations at Poker Flat, Ft. Yukon (F), and Coldfoot (C).

(angle with the vertical) as determined by post-flight analysis of horizon sensor and magnetometer data. Above 70 km the atmospheric drag is minimal and the payload attitude remains constant due to the roll stabilization at 5 Hz. Near 95 km the angle between roll axis and velocity vector (angle of attack) was 35° on upleg and 90° on downleg. The payload orientation and cross-sectional area have an effect on payload charging and the sampling of neutral and charged particles by the probes in the front and back as discussed below.

Major ground-based support was provided by the Poker Flat Incoherent Scatter Radar (PFISR) (Nicolls and Heinselman, 2007) and the sodium and Rayleigh lidars at PFRR (Collins et al., 2011). In this paper, we concentrate on de-
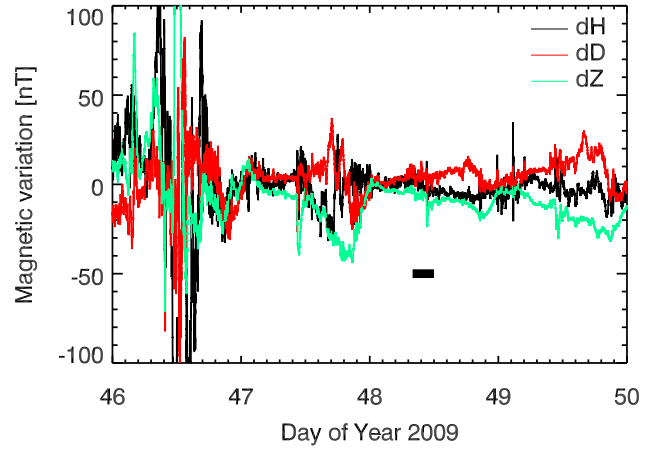

Figure 3. Magnetometer measurements at Poker Flat for 15–19 February 2009 (day 46–50). The period of radar and rocket observations discussed in this paper occurred on day 48, indicated by the black bar. Only very small disturbances can be seen around magnetic midnight at day 48.47.

tailed comparisons between the rocket probe profiles and the electron densities obtained by the incoherent scatter radar. In Fig. 2 the horizontal sampling is projected on a map of central Alaska. PFISR was configured with five beams (numbers 1–5; beam 1 was vertical). The four rocket trajectories are indicated by the long lines originating near beam 1 and labeled with numbers 76 through 79. The horizontal dashes indicate 95 km altitude.

The rocket campaign took place in the middle of the last solar minimum. The geomagnetic conditions were very quiet during the launch day. The planetary Kp index was zero for ∼ 18 h from 00:00 UT until 21:00 UT. The magnetogram for PFRR is shown in Fig. 3 for 15–19 February 2009 (days 46–50). It can be seen that conditions were disturbed on day 46, but variations were of the order of only 10 nT during the launch period on day 48 indicated by the black bar.

The magnetic field was similarly quiet or even quieter than during the sporadic E observations by Turunen et al. (1993) with the European Incoherent Scatter Radar. During the quiet periods, EISCAT meridional electric fields were fluctuating by 5 to 10 mV m^{-1}. PFISR data provided density estimates, but the backscatter signal was too low for estimating electric fields. We assume that the electric field probably did not exceed the quiet time values reported by Turunen et al. (1993) and had probably only a small influence on the formation of Es.

3 Observations

Figure 4 summarizes the most relevant rocket observations in our context of sporadic E. The nose-tip probe on the first instrumented flight, 41.078, launched at 10:29 UT (first panel, blue line), observed a narrow sporadic E layer at 95 km, at
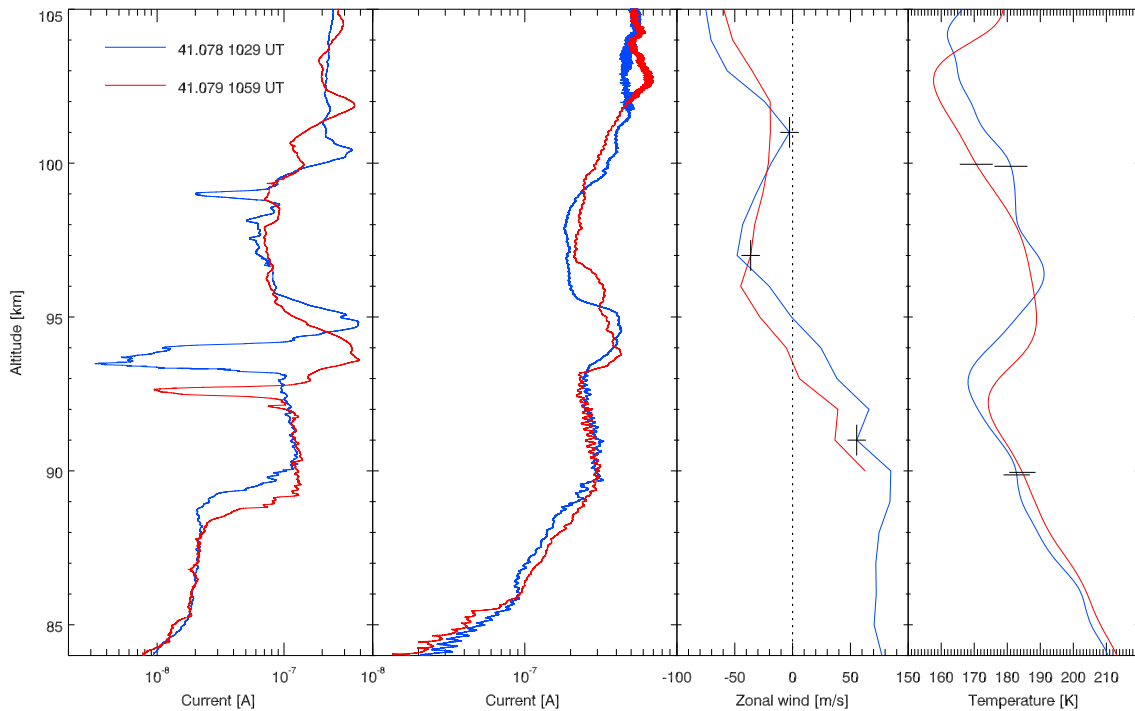
Figure 4. From left to right: nose-tip probe electron currents (ram, upleg), CONE electron probe currents (ram, downleg), zonal winds (upleg), and CONE neutral temperatures (downleg) for missions 41.078 (blue) and 41.079 (red). Typical wind and temperature errors are indicated by black bars.

the same altitude at which a zonal wind node was seen with the chemical releases (third panel). Thirty minutes later, during flight 41.079, the layer had descended about 1 km (red line), as had the wind node. The temperature profiles show a similar downward trend of the local temperature minima (last panel), as does the E-region ledge around 89 km. Due to changing lower atmosphere winds and launch azimuth adjustments, the two instrumented rockets followed slightly different paths through the atmosphere. However, as indicated in Fig. 2, the horizontal deviation between the two flights was only ~ 10 km on upleg and about ~ 20 km on downleg.

The current collected by the nose-tip probe ($+5$ V DC bias) on upleg is a good relative measurement of negative charge density (electrons and small negative ions), as has been demonstrated by comparisons with radio wave propagation measurements (Goldberg et al., 1997; Croskey et al., 2004, 2006) and incoherent scatter radar measurements (Friedrich et al., 2006). For this experiment we are able to convert the probe currents to electron densities matching the PFISR measurements (see below). High-resolution nose-tip probe currents in the D and E regions, ranging from 10^{-10} to 4×10^{-7} A, were obtained from 40 km upward. Notice the close agreement of the background current for the two flights in the upper D region and lower E region. The small-scale fluctuations attributed to mesospheric neutral turbulence were discussed in Lehmacher et al. (2011).

Significant electron depletions appear just below the enhancements, around 94 km (Fig. 4, first panel). The currents were only 10 % or less of the background values. Since these are measurements made by the nose-tip probe on upleg, the depletions were measured before the enhancements.

A second sporadic E layer was crossed first near 100.5 km (left panel, blue line), which had almost disappeared during the next flight (red line), while a third enhancement was present near 102 km. However, the layer structure is less clear in this altitude region, as can also be seen in the radar observations (see below). Therefore, we concentrate on the lower layer in the 95 km region.

The second panel displays the currents for each payload observed by the CONE electron probes on downleg. These probes were also biased with constant $+5$ V but collected about 3 times more current than the nose-tip probes due to different surface area and geometry. The general features of the profiles are similar to the upleg measurements; however, the narrow layers, depletions, and steep gradients are substantially smeared out or not visible at all. We ascribe this response to the unusually shallow angle with which the payloads entered the atmosphere, which in turn led to significant wake effects, and possibly also higher payload charging. We include these measurements since they demonstrate how important the position and orientation of the probe are, even for the collection of mobile electrons. Nevertheless, we note that the altitudes of the Es near 95 km are similar for upleg and
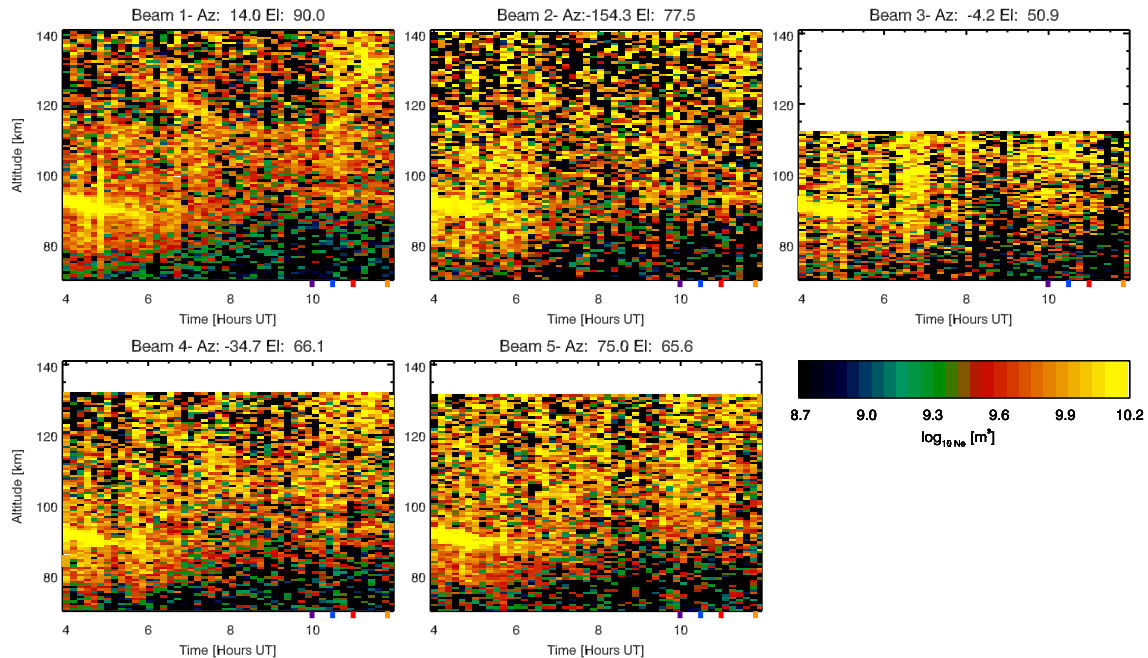
Figure 5. Electron densities observed with PFISR. The times of the four rocket launches (41.076, 78, 79, 77) are marked with the colored ticks at the bottom.

downleg, which gives us an indication of the extent of the layer.

Figure 5 shows PFISR electron densities obtained for the E region with 10 min integrations and 750 m range resolution for all five beams within the observation period between 04:00 and 12:00 UT. The lowest detectable values were 5×10^8 m^{-3}, which was also a typical error estimate for the densities. Several faint layers passed through the radar beam within the 8 h observation period. A strong layer was obvious between 04:00 and 06:00 UT, which coincided with an apparent enhancement in the sodium layer (Collins et al., 2011). This event occurred early in the night before the rockets could be launched. The launch of the rocket salvo was triggered by perturbations in the topside of the sodium layer near 100 km as seen by lidar (Lehmacher et al., 2011). The observation of Es was fortuitous, and radar electron densities helped us in calibrating the fixed-bias electron probe data. In the color image of the radar electron densities, a weak, narrow layer can be traced by eye in several beams as a faint descending line after about 08:00 LT until the end of the observations, when the layer is near 93 km. Although not very prominent in the radar data, we suggest that it is the same layer as seen in the rocket observations.

We again point out the very quiet conditions and very low ionospheric densities during that night. After 10:00 UT, auroral ionization caused higher background electron densities, which can be seen as the brighter pixels in the vertical and northward beams (beams 1 and 3). At this time, which

is around local magnetic midnight, the magnetometer registered stronger perturbations (Fig. 3).

Figure 6 illustrates the development of the horizontal wind components (top panel) over the 2 h period of the rocket observations. Features below 100 km clearly exhibit downward phase propagation. The zonal wind nodes descend at a rate of $-1.3 (\pm 0.3)$ km h^{-1}, characteristic for long-period gravity waves. Based on the hodographs, Lehmacher et al. (2011) identified two major wave motions with periods of 12 and 8 h and vertical wavelengths of 30 and 10 km, respectively.

The bottom panel shows the PFISR electron densities for beam 1 during the time of the rocket observations. Even with the guidance from Fig. 5, the sporadic layer near 95 km is difficult to identify. We performed a spline fit to each radar profile and marked the strongest local maximum in the relevant region with a diamond as our estimated layer altitude. Compared with the zonal wind node (descending black line), it appears that after 11:00 UT the layer remains about 1 km above the wind line. The blue and red rocket profiles are shifted in time and scaled to match the electron densities (see also Fig. 2 in Lehmacher et al., 2011). Background densities are 8×10^9 m^{-3} and layer peak densities are 3 to 4×10^{10} m^{-3}, which is low compared to many other Es measurements.

Evidently, the radar data are noisier than the rocket data and the Es layer is difficult to make out in the individual radar profiles. Weak sporadic layers may be patchy, and so electron densities vary in time and with beam direction. However, the slow descent of the layer and the matching wind nodes
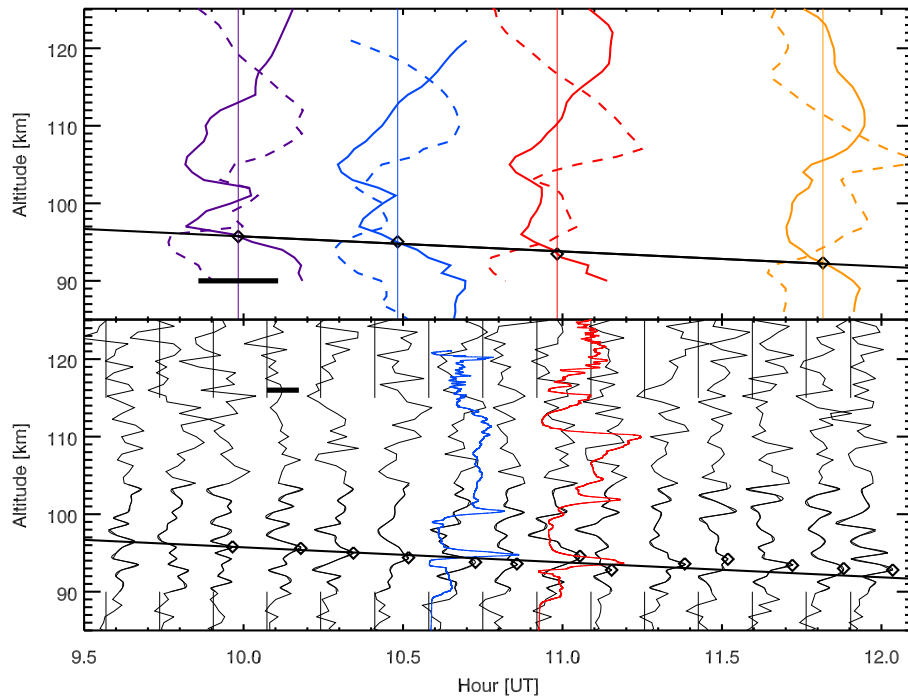
Figure 6. Top: zonal and meridional wind profiles (solid and dashed lines, respectively) from all four flights shifted according to the launch time (41.076 purple, 41.078 blue, 41.079 red, 41.077 yellow). The black bar at the first profile represents $\pm 50\,\mathrm{m\,s^{-1}}$. The slanted line is a linear best fit (slope $-1.3(\pm 0.3)\,\mathrm{km\,h^{-1}}$) to the zonal wind node in the 95 km region. Bottom: vertical profiles of electron density from PFISR (black) and nose-tip probes (blue and red) shifted in time. The scale is linear and the black bar at the fourth profile represents $1 \times 10^{10}\,\mathrm{m^{-3}}$. Error estimates for PFISR are 1 to $6 \times 10^{9}\,\mathrm{m^{-3}}$, increasing with altitude. The nose-tip probe profiles are scaled to match the radar-derived densities in the region below 100 km. The diamonds mark the strongest local maximum near 95 km, descending in altitude (best fit slope $-0.3(\pm 0.5)\,\mathrm{km\,h^{-1}}$). The straight line is again the fit to the wind nodes from the upper panel and is shown for comparison with the electron density structure.

distributed over a 2 h period are significant observations in the context of previous Es and wind measurements.

4   Discussion

4.1   Sporadic E layers

It was first suggested by Nygren et al. (1984) that, at auroral latitudes ($> 60°$), sporadic E layers can be formed by the action of the electric field alone, since the wind shear necessary for the Whitehead mechanism is less effective (Eq. 1), in particular below 110 km altitude.

Kirkwood and von Zahn (1991) studied the role of auroral electric fields in simulations and comparisons with EISCAT observations and found that metallic sporadic layers can be formed between 90 and 105 km when the electric field is westward or southward to southeastward. Electric field effects can be much stronger; for example $E/B \sim (5\,\mathrm{mV\,m^{-1}}/0.05\,\mathrm{mT}) \sim 100\,\mathrm{m\,s^{-1}}$, while disturbed conditions can have horizontal fields of $40\,\mathrm{mV\,m^{-1}}$ or more. Metallic ion lifetimes are of the order of 10 min at 94 km,

which requires persistent wind shears to maintain a layer, when formed by the wind shear mechanism.

Similar calculations were presented by Bristow and Watkins (1991) and supplemented with measurements through steering the Sondrestrom radar by which they could determine the horizontal extent of several Es layers (Bristow and Watkins, 1993).

Kirkwood and von Zahn (1993) refined their analysis and found that a $60\,\mathrm{m\,s^{-1}}$ tidal wind requires 2–3 h to form a 2 km thin layer, which is "dumped" near 93 km altitude. The narrowest layers were generated for a combination of a strong wind and weak 2 to $5\,\mathrm{mV\,m^{-1}}$ southward electric fields. They also found that the shape of the layer is more symmetric under the action of both wind and electric field. These results based on simulations closely resemble our observations.

Figure 7 shows the vertical ion drift as estimated from the observed wind shear for flight 41.078 and Eq. (1). The wind components were rotated from geographic coordinates to geomagnetic coordinates. We used the measured neutral densities from the CONE ionization gauge to estimate the ion collision frequency. The dotted blue line shows the vertical ion drift for the wind profile and zero electrical field. The vertical
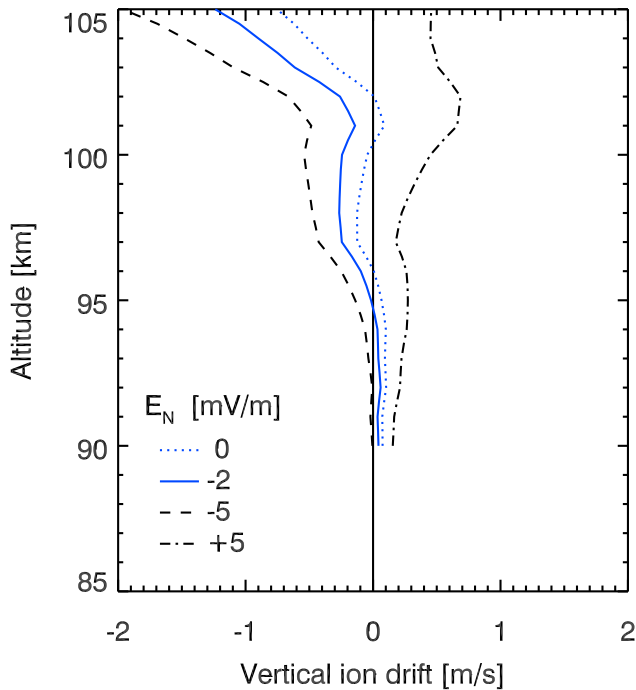
Figure 7. Vertical ion drift as calculated based upon the observed wind shear from flight 41.078 and different meridional electric fields.

ion drifts are very small ($10\,\mathrm{cm\,s^{-1}}$) and convergence times for a 1 km layer are of the order of hours (Haldoupis, 2011), which requires a persistent wind shear to form and maintain the layer. Note that the horizontal wind shear is westward and generates the correct convergence; however, the condition $v_{iz} = 0$ is met near 96 km and not near 95 km.

The additional lines add a northward electric field of -2 (solid), -5 (dashed), and $+5\,\mathrm{mV\,m^{-1}}$ (dash-dotted). Apparently, a small southward field is sufficient to shift the convergence height to 95 km, in agreement with the data and the simulations by Kirkwood and von Zahn (1993). A northward electric field would not create a layer.

We have neglected the influence of the vertical wind on the ion drift (see Williams et al., 2006). This may be justified since the wind pattern is described well by a large-scale gravity wave, for which the zonal and vertical wind components are in phase, i.e., in the zonal wind node the vertical wind is also zero. Figure 6 indicates that the descent of the layer slows after about 11:30 UT. This could be due to the increasing collision frequency and larger influence of ambipolar diffusion; however, beam 2 in Fig. 5 shows enhanced densities until 12:00 UT, the end of the observations.

While Kirkwood and von Zahn (1993) did not find such a clear case in their data of wind shear playing the leading role in the formation of Es, our data indicate that, under very quiet conditions, a sporadic E layer can be produced mainly by the wind shear process, but even minimal electrical fields may be relevant at auroral latitudes.

4.2 Electron biteouts

The deep depletions ("biteouts") just below the sporadic layer are striking features in the electron current profiles (Fig. 4). Just like the sporadic layers, the biteouts appear to follow the downward motion of the zonal wind node.

What could be the cause of such biteouts? First we consider an overall depletion in plasma density, both electrons and ions. The background molecular ions (O_2^+, NO^+) are assumed to be in equilibrium between ionization and recombination. It is also commonly assumed that metallic ions and additional electrons are responsible for the sharply enhanced sporadic layer, in which fast recombination would reduce the molecular ion density.

This effect has been observed directly by ion mass spectrometers (Zbinden et al., 1975; Roddy et al., 2004) and by comparing ion and electron density profiles (Williams et al., 2006). However, this cannot explain the spatial separation of enhanced layer and biteout, since the stronger recombination occurs within the sporadic layer.

Next we consider the formation of a layer of negatively charged particles. Kirkwood and von Zahn (1991) argued that in the electric field action that carries positive ions downward, negative dust particles would be carried upward. However, in our case, wind shear convergence maintaining the positive ion layer would result in divergence for negative ions. The lack of additional information, e.g., for ions, particles, or local electric fields, does not allow us to speculate further as to why the biteout regions appear closely coupled to the Es layer.

On the other hand, it is now well accepted that a broad distribution of meteoric "dust" or "smoke" particles exists in the mesosphere, which are generated by meteor ablation and subsequent chemical and microphysical processes (Hunten et al., 1980).

Mathews (1987) discusses the importance of neutral dust at the "dumping" region for sporadic E around 90 km and estimates the electron attachment rate to neutral dust particles. Beatty et al. (1989) and Kirkwood and von Zahn (1991) pointed out the interaction between dust layers, sporadic E, and neutral metal layers, and that the presence of a charged dust layer would reduce the electric conductivity parallel to the magnetic field and result in charge separation and polarization electric fields. Plane et al. (2014) find that, above the atomic oxygen ledge (typically 88–90 km), negatively charged dust particles of radii < 1 nm (and which contain silicon) are abundant and predominant over negative molecular ions.

The nose-tip probe will generally not detect the relatively heavy dust particles (1000–10 000 amu), since they are being deflected in the supersonic air flow around the payload rather than attracted by the probe electric field. This is well known from flights during polar summer, when dusty ice particles (between 80 and 90 km) give rise to visible noctilucent clouds and polar mesospheric summer echoes observed by

radar. A recent measurement of associated electron biteouts under polar latitude summer conditions with the same nose-tip probe experiment is discussed in Croskey et al. (2004). Nosetip probe currents ranged from 10^{-9} A in the biteout region to 10^{-7} A in the unperturbed background, which are quite similar to the values presented here but about 10 km lower in altitude. The payload carried additional instrumentation that found clear evidence for negatively charged particles in the biteout regions.

Friedrich et al. (2012) present recent rocket observations from December 2010 over Andøya, Norway, which included measurements of negative dust particles with the ECOMA instrument between 80 and 95 km (Rapp et al., 2005), as well as simultaneous electron and ion measurements. Based on observations and supported by simplified ion chemistry, they conclude that dust layers are associated with electron deficits.

A third possibility for the low electron current is negative payload charging, which would lower the collection efficiency of the positively biased nose-tip probe. DC probes often collect significantly less current than predicted by Langmuir probe theory (Piel et al., 2001). This also applies to the nose-tip probe as shown for daytime and nighttime conditions (Friedrich et al., 1997), but the relative density profiles can be normalized with the help of other techniques (e.g., Friedrich et al., 2006).

Friedrich et al. (2013) show profiles of a wide sporadic E layer between 95 and 100 km observed by the radio propagation technique, which provides an absolute measurement of electron density, together with data from a payload potential monitor for the same polar night flight in December 2010 mentioned above. The payload potential is generally negative, between -2 and -1 V, and about 0.5 V more negative within the sporadic layer. However, Friedrich et al. (2013) show that this variation had no significant effect on the in situ DC probe measurements.

Barjatya and Swenson (2006) report rocket measurements of a sporadic E layer near 92 km and suggest that triboelectric payload charging had significantly decreased the current collected by a DC electron probe when compared to simultaneous RF impedance probe measurements. In our measurements we do not observe depressed electron currents in the sporadic E-layer peak.

Unfortunately, our instrumentation did not include dust detectors, ion probes, or RF electron probes, which would have provided very valuable data in the biteout regions. However, based on similar observations with the same probe in the polar summer mesosphere, our data suggest that the biteout regions below the sporadic E layers were indeed depletions of free electrons. While more recent experiments find evidence for layering effects in charged dust particles, our observations show, for the first time, electron biteouts in connection with sporadic E. The circumstance of very low ionization may have played a role in our observations, but more comprehensive measurements are needed to shed light on the connection between dust particles and sporadic E, which has been a topic of discussion for over 30 years.

5 Summary and conclusions

We have presented in situ and radar measurements of E-region sporadic layers during nighttime and very quiet conditions at auroral latitudes. Here we summarize our most significant findings.

1. Persistent wind shears were likely the leading cause of Es formation at this relatively low altitude of about 95 km. The wind shear region was also responsible for the downward motion of the layer. Our observations are unique and perhaps somewhat surprising, since there are few measurements like ours and the neutral wind is generally considered inefficient at high latitudes. Based on our analysis, we infer that the convection electric fields were very small or negligible. Our results, however, are consistent with earlier incoherent scatter radar observations under very quiet conditions and also with modeling results.

2. Deep electron biteouts below the sporadic E layers at nighttime are a new observation. By analogy with similar biteouts observed in the polar summer mesosphere and evidence from other experiments, we suggest that the biteouts are electron depletions and possibly associated with a layer of negatively charged dust particles that our probe cannot collect. We find support in recent simultaneous measurements of negative dust particles and electron densities, as well as in modeling results showing a significant fraction of negatively charged dust particles above 90 km. The wind shear theory does not offer an explanation why the depleted layer seems connected to the Es layer. We recommend future experiments with the capability to observe electrons, light ions, and charged dust, with launches done in quiet nighttime conditions to help in resolving the questions surrounding sporadic E and dust layers.

References

Axford, W. I.: The formation and vertical movement of dense ionized layers in the ionosphere, J. Geophys. Res., 68, 769–779, 1963.

Barjatya, A. and Swenson, C. M.: Observations of Triboelectric Charging Effects on Langmuir-Type Probes in Dusty Plasma, J. Geophys. Res., 111, A10302, doi:10.1029/2006JA011806, 2006.

Beatty, T. J., Collins, R. L., Gardner, C. S., Hostetler, C. A., Sechrist Jr., C. F., and Tepley, C. A.: Simultaneous radar and lidar observations of sporadic E and Na layers at Arecibo, Geophys. Res. Lett., 16, 1019–1022, 1989.

Bristow, W. A. and Watkins, B. J.: Numerical simulation of the formation of thin ionization layers at high latitudes, Geophys. Res. Lett., 18, 404–407, 1991.

Bristow, W. A. and Watkins, B. J.: Incoherent scatter observations of thin ionization layers at Sondrestrom, J. Atmos. Terr. Phys., 55, 873–894, 1993.

Chimonas, G. and Axford, W. I.: Vertical movement of temperate zone sporadic E layer, J. Geophys. Res., 73, 111–117, 1968.

Collins, R. L., Lehmacher, G. A., Larsen, M. F., and Mizutani, K.: Estimates of vertical eddy diffusivity in the upper mesosphere in the presence of a mesospheric inversion layer, Ann. Geophys., 29, 2019–2029, doi:10.5194/angeo-29-2019-2011, 2011.

Croskey, C. L., Mitchell, J. D., Goldberg, R. A., Blix, T. A., Rapp, M., Latteck, R., Friedrich, M., and Smiley, B.: Coordinated investigation of plasma and neutral density fluctuations and particles during the MaCWAVE/MIDAS summer 2002 program, Geophys. Res. Lett., 31, L24S08, doi:10.1029/2004GL020169, 2004.

Croskey, C. L., Mitchell, J. D., Friedrich, M., Schmidlin, F. J., and Goldberg, R. A.: In-situ electron and ion measurements and observed gravity wave effects in the polar mesosphere during the MaCWAVE program, Ann. Geophys., 24, 1267–1278, doi:10.5194/angeo-24-1267-2006, 2006.

Friedrich, M., Torkar, K. M., Goldberg, R. A., Mitchell, J. D., Croskey, C. L., and Lehmacher, G.: Comparison of plasma probes in the lower ionosphere, Proc. 13th ESA Symp. on Rocket and Balloon Programmes and Related Research, land, Sweden, 26–29 May 1997, ESA SP-397, 381–386, 1997.

Friedrich, M., Torkar, K. M., Lehmacher, G. A., Croskey, C. L., Mitchell, J. D., Kudeki, E., and Milla, M.: Rocket and Incoherent Scatter Radar Common-Volume Electron Measurements of the Equatorial Lower Ionosphere, Geophys. Res. Lett., 33, L08807, doi:10.1029/2005GL024622, 2006.

Friedrich, M., Rapp, M., Blix, T., Hoppe, U.-P., Torkar, K., Robertson, S., Dickson, S., and Lynch, K.: Electron loss and meteoric dust in the mesosphere, Ann. Geophys., 30, 1495–1501, doi:10.5194/angeo-30-1495-2012, 2012.

Friedrich, M., Torkar, K. M., Hoppe, U.-P., Bekkeng, T.-A., Barjatya, A., and Rapp, M.: Multi-instrument comparisons of D-region plasma measurements, Ann. Geophys., 31, 135–144, doi:10.5194/angeo-31-135-2013, 2013.

Giebeler, J., Lübken, F.-J., and Nägele, M.: CONE – a new sensor for in situ observations of neutral and plasma density fluctuations, Proc. 11th ESA Symp. Europ. Rocket Balloon Progr., Montreux, Switzerland, ESA SP-355, 311–318, 1993.

Goldberg, R. A., Lehmacher, G. A., Schmidlin, F. J., Fritts, D. C., Mitchell, J. D., Croskey, C. L., Friedrich, M., and Swartz, W. E.: Equatorial dynamics observed by rocket, radar, and satellite during the CADRE/MALTED campaign. 1. Programmatics and small-scale fluctuations, J. Geophys. Res., 102, 26179–26190, 1997.

Haldoupis, C.: A tutorial review on sporadic E layers, in: Aeronomy of the Earth's Atmosphere and Ionosphere, edited by: Abdu, M. A., Pancheva, D., and Bhattacharyya, A., Springer, Dordrecht, the Netherlands, 381–394, doi:10.1007/978-94-007-0326-1_29, 2011.

Havnes, O., Trøim, J., Blix, T., Mortensen, T. W., Nuheim, L. I., Thrane, E., and Tønnesen, T.: First detection of charged dust particles in the Earth's mesosphere, J. Geophys. Res., 101, 10839–10848, 1996.

Heinselman, C. J., Thayer, J. P., and Watkins, B. J.: A high-latitude observation of sporadic sodium and sporadic E-layer formation, Geophys. Res. Lett., 25, 3059–3062, 1998.

Hunten, D. M., Turco, R. P., and Toon, O. B.: Smoke and dust particles of meteoric origin in the mesosphere and stratosphere, J. Atmos. Sci., 37, 1342–1357, 1980.

Kato, S., Aso, T., Horiuchi, T., Nakamura, J., and Matsuoka, T.: Sporadic-E formation by wind shear, comparison between observation and theory, Radio Sci., 7, 359–362, 1972.

Kirkwood, S. and Nilsson, H.: High-latitude sporadic-E and other thin layers – the role of magnetospheric electric fields, Space Sci. Rev., 91, 579–613, 2000.

Kirkwood, S. and von Zahn, U.: On the role of auroral electric fields in the formation of low altitude sporadic-E and sudden sodium layers, J. Atmos. Terr. Phys, 53, 389–407, 1991.

Kirkwood, S. and von Zahn, U.: Formation mechanisms for low-altitude Es and their relationship with neutral Fe layers: Results from the METAL campaign, J. Geophys. Res., 98, 21549–21561, 1993.

Knappmiller, S., Robertson, S, Sternovsky, Z., and Friedrich, M.: A rocket-borne mass analyzer for charged aerosol particles in the mesosphere, Rev. Sci. Instr., 79, 104502, doi:10.1063/1.2999580, 2008.

Larsen, M. F.: Winds and shears in the mesosphere and lower thermosphere: Results from four decades of chemical release wind measurements, J. Geophys. Res., 107, A8, doi:10.1029/2001JA000218, 2002.

Lehmacher, G. A., Scott, T. D., Larsen, M. F., Bilén, S. G., Croskey, C. L., Mitchell, J. D., Rapp, M., Lübken, F.-J., and Collins, R. L.: The Turbopause experiment: atmospheric stability and turbulent structure spanning the turbopause altitude, Ann. Geophys., 29, 2327–2339, doi:10.5194/angeo-29-2327-2011, 2011.

Lynch, K. A., Gelinas, L. J., Kelley, M. C., Collins, R. L., Widholm, M., Rau, D., MacDonald, E., Liu, Y., Ulwick, J., and Mace, P.: Multiple sounding rocket observations of charged dust in the polar winter mesosphere, J. Geophys. Res., 110, A03302, doi:10.1029/2004JA010502, 2005.

MacLeod, M. A.: Sporadic E Theory. I. Collision-Geomagnetic Equilibrium, J. Atmos. Sci., 23, 96–109, 1966.

Mathews, J. D.: Some aspects of metallic ion chemistry and dynamics in the mesosphere and thermosphere, Handbook for MAP, 25, 228–254, 1987.

Mathews, J. D.: Sporadic E: current views and recent progress, J. Atmos. Solar-Terr. Phys., 60, 413–435, 1998.

Nicolls, M. J. and Heinselman, C. J.: Three-dimensional measurements of traveling ionospheric disturbances with the Poker Flat Incoherent Scatter Radar, Geophys. Res. Lett., 34, L21104, doi:10.1029/2007GL031506, 2007.

Nygren, T., Jalonen, L., Oksman, J., and Turunen, T.: The role of electric field and neutral wind direction in the formation of sporadic E-layers, J. Atmos. Terr. Phys., 46, 373–381, 1984.

Piel, A., Hirt, M., and Steigies, C. T.: Plasma diagnostics with Langmuir probes in the equatorial ionosphere: I. the influence of surface contamination, J. Phys. D Appl. Phys., 34, 2643–2649, 2001.

Plane, J. M. C., Saunders, R. W., Hedin, J., Stegman, J., Khaplanov, M., Gumbel, J., Lynch, K. A., Bracikowski, P. J., Gelinas, L. J., Friedrich, M., Blindheim, S., Gausa, M., and Williams, B. P.: A combined rocket-borne and ground-based study of the sodium layer and charged dust in the upper mesosphere, J. Atmos. Solar-Terr. Phys., 118, 151–160, doi:10.1016/j.jastp.2013.11.008, 2014.

Rapp, M., Hedin, J., Strelnikova, I., Friedrich, M., Gumbel, J., and Lübken, F.-J.: Observations of positively charged nanoparticles in the nighttime polar mesosphere, Geophys. Res. Lett., 32, L23821, doi:10.1029/2005GL024676, 2005.

Roddy, P. A., Earle, G. D., Swenson, C. M., Carlson, G. G., and Bullett, T. W.: Relative concentrations of molecular and metallic ions in midlatitude intermediate and sporadic-E layers, Geophys. Res. Lett., 31, L19807, doi:10.1029/2004GL020604, 2004.

Smith, L. G. and Mechtly, E. A.: Rocket observations of sporadic-E layers, Radio Sci., 7, 367–376, 1972.

Smith, L. G. and Miller, K. L.: Sporadic-E layers and unstable wind shears, J. Atmos. Terr. Phys., 42, 45–50, 1980.

Turunen, T., Nygren, T., and Huuskonen, A.: Nocturnal high-latitude E-region in winter during extremely quiet conditions J. Atmos Terr. Solar-Phys., 55, 783–795, 1993.

Ulwick, J. C., Baker, K. D., Kelley, M. C., Balsley, B. B., and Ecklund, W. L.: Comparison of simultaneous MST radar and electron density probe measurements during STATE, J. Geophys. Res., 93, 6989–7000, 1988.

Wakabayashi, M. and Ono, T.: Multi-layer structure of mid-latitude sporadic-E observed during the SEEK-2 campaign, Ann. Geophys., 23, 2347–2355, doi:10.5194/angeo-23-2347-2005, 2005.

Whitehead, J. D.: The formation of the sporadic E layer in the temperate zones, J. Atmos. Solar-Terr. Phys., 20, 49–58, 1961.

Whitehead, J. D.: Production and prediction of sporadic E, Rev. Geophys. Space Sci., 8, 65–144, 1970.

Williams, B. P., Croskey, C. L., She, C. Y., Mitchell, J. D., and Goldberg, R. A.: Sporadic sodium and E layers observed during the summer 2002 MaCWAVE/MIDAS rocket campaign, Ann. Geophys., 24, 1257–1266, doi:10.5194/angeo-24-1257-2006, 2006.

Zbinden, P. A., Hidalgo, M. A., Eberhardt, P., and Geiss, J.: Mass spectrometer measurements of the positive ion composition in the D- and E-regions of the ionosphere, Planet. Space Sci., 23, 12, 1621–1642, 1975.